

RESEARCH

Open Access



HMGB1 Box A gene therapy to alleviate bleomycin-induced pulmonary fibrosis in rats

Rathasapa Patarat^{1,2}, Suchanart Chuaybudda^{1,2}, Sakawdaurn Yasom^{3*} and Apiwat Mutirangura^{1*}

Abstract

Background Pulmonary fibrosis is characterized by the destruction of normal lung tissue and then replacement by abnormal fibrous tissue, leading to an overall decrease in gas exchange function. The effective treatment for pulmonary fibrosis remains unknown. The upstream pathogenesis of pulmonary fibrosis may involve cellular senescence of the lung tissue. Previously, a new gene therapy technology using Box A of the HMGB1 plasmid (Box A) was used to reverse cellular senescence and cure liver fibrosis in aged rats.

Methods Here, we show that Box A is a promising medicine for the treatment of lung fibrosis. In a bleomycin-induced pulmonary fibrosis model in the male Wistar rats, Student's *t*-test and one-way ANOVA were used to compare groups of samples.

Results Box A effectively lowered fibrous tissue deposits (from 18.74 ± 0.62 to $3.45 \pm 1.19\%$) and senescent cells (from $3.74 \pm 0.40\%$ to $0.89 \pm 0.18\%$) to levels comparable to those of the negative control group. Moreover, after eight weeks, Box A also increased the production of the surfactant protein C (from $3.60 \pm 1.68\%$ to $6.82 \pm 0.65\%$).

Conclusions Our results demonstrate that Box A is a promising therapeutic approach for pulmonary fibrosis and other senescence-promoted fibrotic lesions.

Keywords Idiopathic pulmonary fibrosis, DNA damage, DNA stability, DNA protection, Box a of HMGB1, Youth-DNA-gap, Senescence, Rejuvenation, Gene therapy

Background

Pulmonary fibrosis is a chronic lung disease characterized by defective pulmonary structural remodeling [1]. This remodeling includes excessive irregular fibrous tissue deposition in the extracellular matrix, increased numbers of senescent cells, and loss of normal gas exchange function [2]. Pulmonary fibrosis affects approximately 5 million patients worldwide, and its incidence has sharply increased in recent years due to the COVID-19 pandemic [3]. A meta-analysis revealed that patients who survive severe COVID-19 infection are at risk of developing pulmonary fibrosis disease [4]. Moreover, severe pulmonary fibrosis disease cases have a mortality rate of 50% annually, with a median survival rate of 3 years after diagnosis.

*Correspondence:

Sakawdaurn Yasom
apple.medmicro2013@gmail.com
Apiwat Mutirangura
apiwat.mutirangura@gmail.com

¹Center of Excellence in Molecular Genetics of Cancer and Human Diseases, Department of Anatomy, Faculty of Medicine, Chulalongkorn University, King Chulalongkorn Memorial Hospital, Bangkok 10330, Thailand

²Interdisciplinary Program of Biomedical Sciences, Graduate School, Chulalongkorn University, Bangkok, Thailand

³Department of Microbiology, Faculty of Medicine, Chiang Mai University, Chiang Mai, Thailand



© The Author(s) 2025. **Open Access** This article is licensed under a Creative Commons Attribution-NonCommercial-NoDerivatives 4.0 International License, which permits any non-commercial use, sharing, distribution and reproduction in any medium or format, as long as you give appropriate credit to the original author(s) and the source, provide a link to the Creative Commons licence, and indicate if you modified the licensed material. You do not have permission under this licence to share adapted material derived from this article or parts of it. The images or other third party material in this article are included in the article's Creative Commons licence, unless indicated otherwise in a credit line to the material. If material is not included in the article's Creative Commons licence and your intended use is not permitted by statutory regulation or exceeds the permitted use, you will need to obtain permission directly from the copyright holder. To view a copy of this licence, visit <http://creativecommons.org/licenses/by-nc-nd/4.0/>.

Currently, scientists can identify many pathways responsible for developing pulmonary fibrosis [5]. Cellular senescence has been identified as a common cause of pulmonary fibrosis [6–8]. The accumulation of senescent cells of various cell types in the tissue leads to dysfunction of multiple normal tissue functions and results in excessive production of fibrous tissue, impaired fibrous tissue clearance, decreased proliferation of alveolar cells and/or endothelial cells, and prolonged aggregation of inflammatory cells. Ultimately, pulmonary fibrosis can develop [9, 10]. Currently, the pharmacological targets for pulmonary fibrosis include epigenetic alterations, antifibrogenic agents, fibrolysis agents, and senolytic agents [11–13]. However, effective treatments for pulmonary fibrosis are lacking.

For the last decade, our group has studied a new gene therapy for aging, the Box A portion of the high mobility group Box 1 (Box A of HMGB1 or Box A) protein. Box A provides DNA protection and increases genomic stability [14]. Having functions as molecular scissors, Box A produces youth-DNA-gaps to relieve DNA torsional stress due to DNA double helix denaturation during replication and transcription. Our group has already utilized Box A to treat liver fibrosis in two animal models. We found that administering Box A significantly reduced not only senescent cells but also liver fibrosis to a level comparable to that of the control group [14].

Therefore, Box A could be a novel therapeutic agent for treating pulmonary fibrosis. In this study, we investigated the ability of Box A to alleviate bleomycin-induced pulmonary fibrosis in a rat model. We used this model because the rat that received bleomycin had been shown to develop the pulmonary fibrosis with the pathogenesis and histopathology that mirror those of its human counterpart. These findings demonstrate the potential of Box A for treating pulmonary fibrosis and can be developed into a new treatment for other senescence-induced fibrotic diseases.

Methods

Plasmid construction and preparation

In this study, we used the full-length human Box A sequence of HMGB1 and a scrambled sequence for the plasmid control (PC). The plasmids were subsequently transformed into *Escherichia coli* (DH5 α) (Invitrogen), specifically, NEB $^{\circ}$ 5-alpha competent *E. coli* (New England BioLabs). Transformed cells were grown on LB agar supplemented with ampicillin or chloramphenicol for all plasmid selection. The selected colony was then cultured in LB broth supplemented with 100 μ g/ml ampicillin and incubated on an incubator shaker at 37 $^{\circ}$ C for 16 h. The plasmids were then extracted via a GeneJET Plasmid Maxiprep Kit (Thermo Fisher Scientific) according to the manufacturer's instructions. Sequence fidelity

was confirmed by Sanger sequencing. The full length of human HMGB1 DNA sequence used during the current study is available in the GenBank Nucleotide Repository, accession number: BT020159.

Nanoparticle construction and preparation

To deliver the plasmids into the rat model, each type of plasmid was coated with a Calcium-Phosphate (Ca-P) nanoparticle mixture before administration. Our team prepared the solution at the maximal effective concentration [14–15]. The highest effective plasmid to Ca-P nanoparticle solution ratio for transfection was 5 μ g of plasmid in 100 μ l of Ca-P nanoparticle solution. The Ca-P nanoparticle solution was composed of a mixture of 0.5 M calcium chloride (CaCl $_2$) solution (Merck Millipore), 0.01 M sodium carbonate (Na $_2$ CO $_3$) solution (Merck Millipore), and 0.01 M sodium dihydrogen phosphate monohydrate (NaH $_2$ PO $_4$ ·H $_2$ O) solution (Merck Millipore). The final molar ratio of the CO $_3^{2-}$ /PO $_4^{3-}$ nanoparticle solution was 3:1. We followed these steps to mix the solutions. First, the plasmid DNA-calcium complex was prepared by mixing 16 μ l of CaCl $_2$ solution and 5 μ g of plasmid DNA, with the final volume adjusted to 50 μ l via sterile dH $_2$ O, and the mixture was maintained at room temperature. Second, the plasmid DNA-calcium complex was added to 50 μ l of a mixture of Na $_2$ CO $_3$ and NaH $_2$ PO $_4$ ·H $_2$ O solution (16 μ l) and sterile dH $_2$ O (34 μ l). The final solution contained CaPO $_4$ /plasmid DNA nanoparticles as intended. For the rat model, each plasmid type was calculated based on the rat body weight (100 μ g of plasmid DNA per kg of rat body weight). After calculating the solution, the plasmid DNA was coated with the Ca-P nanoparticle solution described above. Finally, the plasmid DNA-Ca-P nanoparticle mixture was freshly prepared before intraperitoneal administration.

Animal disease models and therapeutic diagram

All animal procedures were reviewed and approved by the Animal Care and Use Committee, Medical Faculty, Chulalongkorn University, Thailand, Approval No. 032/2564. We use G*Power program version 3.1.9.7 to calculate the sample size for this study [16]. We reference the results from recent studies to calculate an appropriate sample size [14, 17–20]. The effect size from the equation [effect size = (Mean1-Mean2)/SDpooled]. The effect size equals 0.36 [14]. The result from the G*Power program suggests that we use at least 36 rats for the total sample size. Then we divided into six equal groups of 6 rats for this experiment.

Thirty-six male Wistar rats (6–8 weeks of age) were purchased from Nomura Siam International, Bangkok, Thailand. After one week of acclimatization, all the animals were housed in a temperature-controlled chamber (25 \pm 0.5 $^{\circ}$ C) with a 12:12-hour light/dark cycle with

a standard diet, and sterilized water was provided *ad libitum*. All the rats were monitored daily and weighed weekly until they reached the desired weight and age. The rats were included in this study and given the individual code only when they reached the desired weight of 300–350 g. The rats of the desired weights were randomly assigned using random number generator to subgroups by a laboratory technician who was blinded to the characteristics of the rats. Thirty-six male Wistar rats were used in this study and were randomly assigned to six subgroups (Fig. 1). For the use of Bleomycin injection, we studied the previously published experiment using Bleomycin as the agent for inducing the pulmonary fibrosis in the rat [21–23].

For the blinding procedure, the first investigator, who labels the rat and gives the individual code, is the only one who knows the treatment allocation, the second investigator assists with the anesthetic procedure, and the third investigator helps with blood collection and organ collection.

After acclimatization and the animal coding, normal saline solution (NSS) or bleomycin was intraperitoneally administered on Day 0, thrice weekly, and stopped on

Day 21 or after nine doses into the vehicle control or the disease model group, respectively.

1. 6-week Vehicle Control group: six rats were given NSS as mentioned earlier. Fourteen days later, the PC-calcium phosphate (100 µg/kg) was administered intraperitoneally (i.p.) once every week for six weeks (Day 35, 42, 49, 56, 63, and 70, the injections being designated at the same time points as groups 2–3).
2. 6-week Disease Model group: As mentioned above, six rats were given bleomycin (15 mg/kg). Fourteen days later, we intraperitoneally administered the PC-calcium Phosphate (100 µg/kg) once every week for six weeks.
3. 6-week Treatment Group: six bleomycin-given rats were intraperitoneally administered with Box A-calcium phosphate (100 µg/kg) once every week for six weeks.
4. 8-week Vehicle Control group: six NSS-injected rats were intraperitoneally given the PC-calcium phosphate (100 µg/kg) once every week for 8 weeks (Day 35, 42, 49, 56, 63, 70, 77, and 84, the

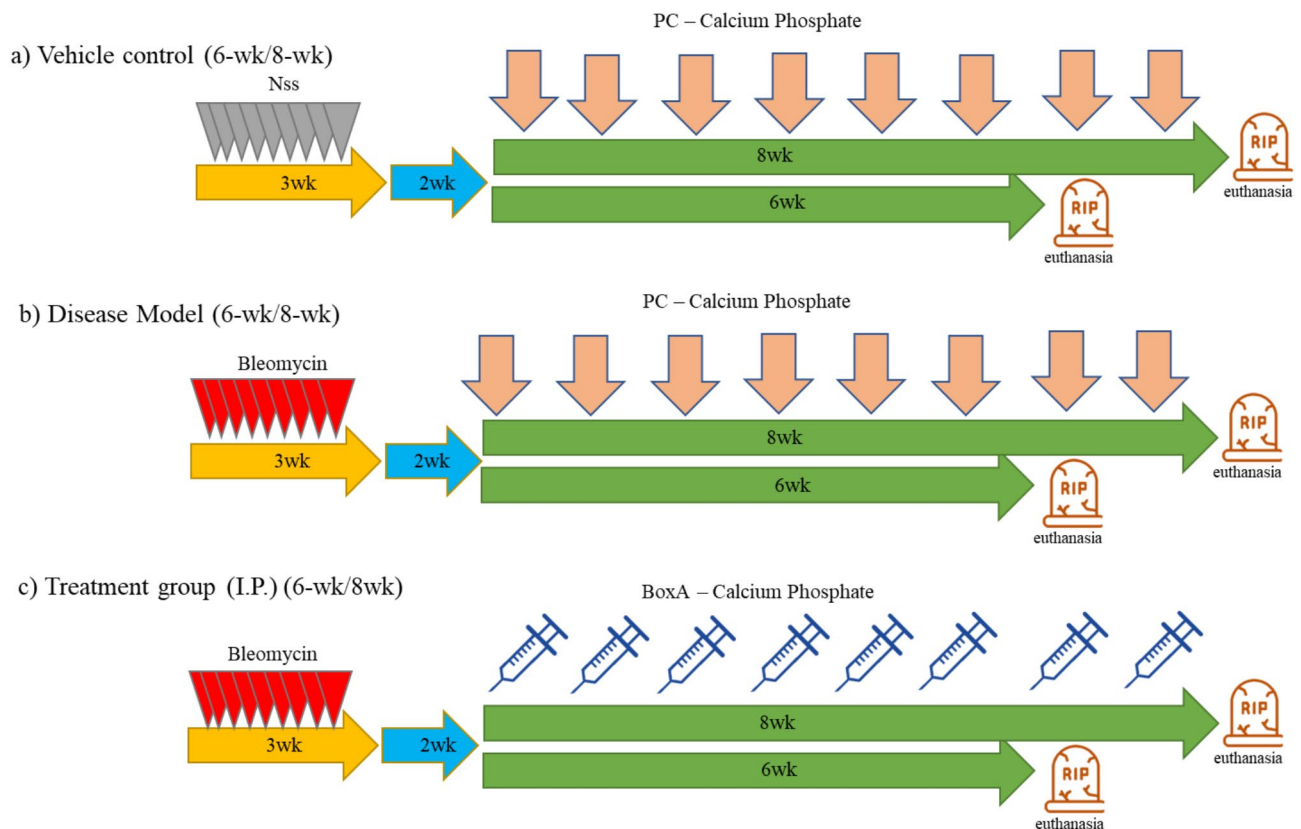


Fig. 1 Schematic diagrams of bleomycin-induced pulmonary fibrosis treatment in a rat model. The rats were given either bleomycin (15 mg/kg/dose, i.p.) or normal saline solution (NSS) at 3 doses/week for 3 weeks, allowed to rest for 2 weeks, and then given either Box A plasmid-calcium-phosphate nanoparticles (Box A) (100 µg/kg/week, i.p.) or plasmid control (PC)-calcium-phosphate nanoparticles (100 µg/kg/week, i.p.), and the injections were continued for either 6 or 8 weeks

administrations being designated at the same time points as groups 5–6).

5. 8-week Disease Model group: six bleomycin-induced rats were intraperitoneally given the PC-calcium phosphate (100 µg/kg) once every week for 8 weeks.
6. 8-week Treatment Group: six bleomycin-induced rats were intraperitoneally given the Box A-calcium phosphate (100 µg/kg) once every week for 8 weeks.

All rats in groups 1–3 and 4–6 were euthanized on Days 77 and 91, respectively.

Detection of blood chemistry and complete blood count

Blood samples from all the rats were collected at the beginning of the acclimatization period, before bleomycin/normal saline was administered, before plasmid/treatment was administered, and just after euthanization. The blood samples were collected and shipped to the Pathology Laboratory Department, Small Animal Hospital, Faculty of Veterinary Medicine, Chulalongkorn University, for analysis of the complete blood count and glucose, creatinine, total protein, albumin, globulin, alanine transaminase, alkaline phosphatase, C-reactive protein, and blood urea nitrogen (BUN) levels. All the blood samples for the complete blood count were measured via a ProCyte Dx analyzer (IDEXX, USA). All blood samples for blood chemistry were measured via a Catalyst One Chemistry analyzer (IDEXX, USA).

Animal euthanization method

The euthanization method is reviewed and approved by the CHULALONGKORN UNIVERSITY ANIMAL CARE AND USE PROTOCOL (CU-ACUP) committee. Detailed euthanization procedure is as follow. At the time point of interest, the appointed rat is sedated first by carefully masked with isoflurane (5% mixed with room air) until observed relaxed muscle tone then continue using an Isoflurane (5% mixed with room air) exposure at a flow rate of 3.5 L/min until one minute after observed that the breathing had stopped. Anesthetic depth is monitored and assessed every minute by observed respiration, muscle tone, pupil, and reflex (such as tail pinch). Then, verify death by an absence of cardio-vascular function for one minute continuously.

SA-β-Gal staining

After euthanization, the rat tissues were immediately dissected and fixed in a fresh fixative buffer; for the SA-β-Gal (senescence-associated- beta-galactosidase) staining method, lungs were fixed in 4% paraformaldehyde (PFA) before being embedded in optimal cutting temperature (OCT) compound (Sakura, Tissue-Tek) and cryosectioned at a thickness of 10 µm. After

rehydration of the lung sections in PBS for 10 min, the sections were subjected to SA-β-gal staining via a Cell Signaling Kit (9860, Beverly, MA, USA) with 15-min of fixation followed by incubation at 37 °C in the staining solution for at least 12 h. Images of the sections were captured via a Leica DM1000 inverted microscope with a color camera. SA-β-gal in lung sections was quantified. The images were analyzed via densitometry. ImageJ software (open source) was used to analyze the area with SA-β-Gal staining.

Histopathological analysis

After euthanization, the rat tissues were immediately dissected and fixed in the fresh fixative buffer. For Masson's trichrome staining, lungs were fixed in 10% neutral buffered formalin for less than 48 h, processed into paraffin blocks, and cut into 5-µm sections. The slides were subjected to Masson's trichrome staining according to standard procedures for histopathological analysis. The Masson trichrome-stained slides were captured via a Leica DM1000 inverted microscope with a color camera. The images were evaluated for fibrous tissue accumulation and degree of fibrosis in the lung according to the standard histopathological analysis of pulmonary fibrosis. ImageJ software (open source) was used to analyze the densitometry of the fibrotic tissue.

Immunohistochemistry (IHC) staining

After euthanization, the rat tissues were immediately dissected and fixed in the fresh fixative buffer. For IHC staining, lungs were fixed in 10% neutral buffered formalin for less than 48 h, processed into paraffin blocks, and cut into 5-µm sections. The immunohistochemistry (IHC) procedure was as follows: deparaffinized at 65 °C for 15 min, rehydrate in descending alcohol series, rinse with hydrogen peroxide, rest for antigen retrieval in 10 mM sodium citrate buffer (pH 6.0) at 100 °C for 20 min, rinse with PBS, and then block with 2% FBS. Then, the sections were incubated with either (1:50) rabbit anti-SFTPC antibody (ABC99, Abcam®) or (1:500) rabbit anti-DYKDDDDK tag (FLAG) antibody (#14793, Cell Signaling) at room temperature overnight. Afterwards, the slides were rinsed with PBS and incubated with an HRP-linked anti-rabbit IgG antibody (7074 V, Cell Signaling®) at 30 °C for 1 h. Then, the slides were washed with PBS and incubated with ABC solution at 30 °C for 30 min. The slides were then washed in PBS, incubated with DAB substrate (Merck®) at room temperature for 10 min, and then rinsed with tap water. Moreover, hematoxylin was used to counterstain slides with an anti-DYKDDDDK tag. However, none of the anti-SFTPC slides were counterstained. Finally, the sections were captured via a Leica

DM1000 inverted microscope with a color camera. The images were analysed via densitometry to quantify immunohistochemical staining in lung sections. ImageJ software (open source) was used to analyze the area with positive staining.

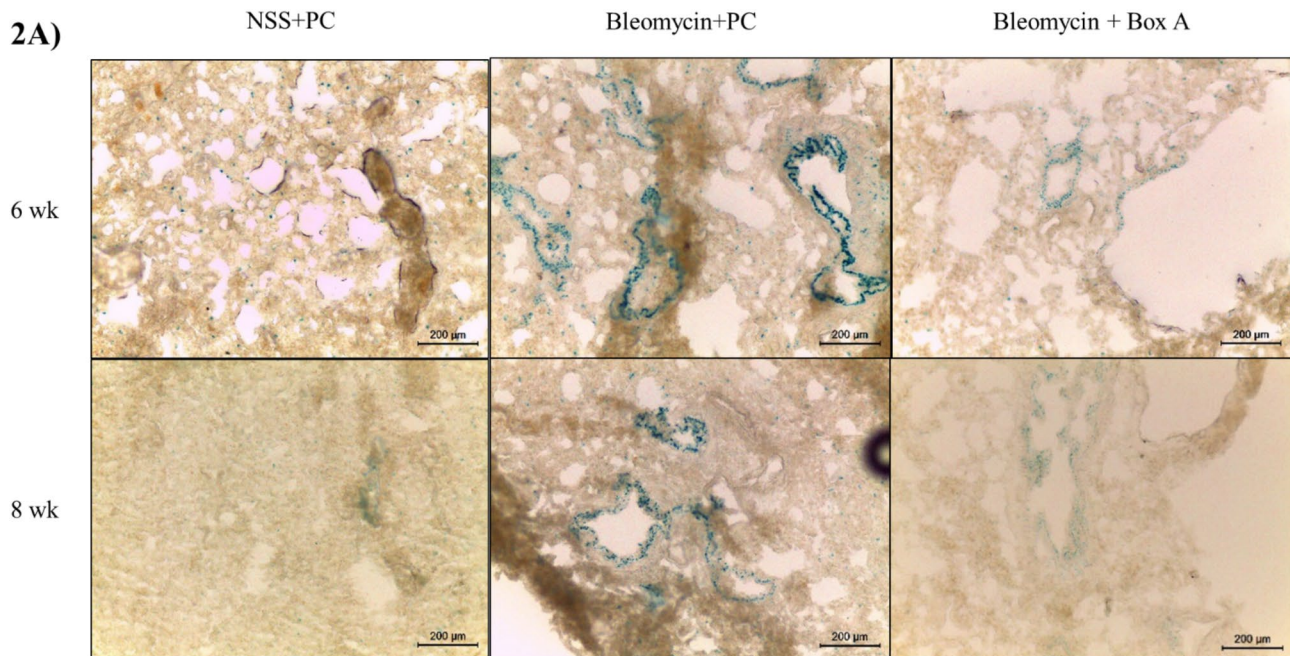
Statistics

The data were analyzed for their distribution before the appropriate analysis tools were selected. Student's *t*-test was used to compare two sets of samples and one-way ANOVA was used to compare multiple groups of samples. Statistical analyses were performed with GraphPad Prism V9.5 for Windows (GraphPad Software, Inc.).

Results

Effectiveness of Box A in reducing senescence in bleomycin-induced pulmonary fibrosis

Thirty-six male Wistar rats were included and randomized in this experiment. After treating rats with bleomycin-induced pulmonary fibrosis with Box A protein following our experimental protocol (Fig. 1), we euthanized the rats, harvested the lung tissue for senescence-associated beta-galactosidase staining, and analyzed the area of staining. We calculated the area of senescence for each group (Fig. 2). The groups that received NSS+ plasmid control, bleomycin+plasmid control, or bleomycin+Box A for 6 weeks exhibited senescence areas encompassing $0.36 \pm 0.04\%$, $3.8 \pm 0.19\%$, and $1.04 \pm 0.21\%$ (mean \pm SD) of the total tissue area, respectively. The



2B) Senescence-Associated beta-Galactosidase

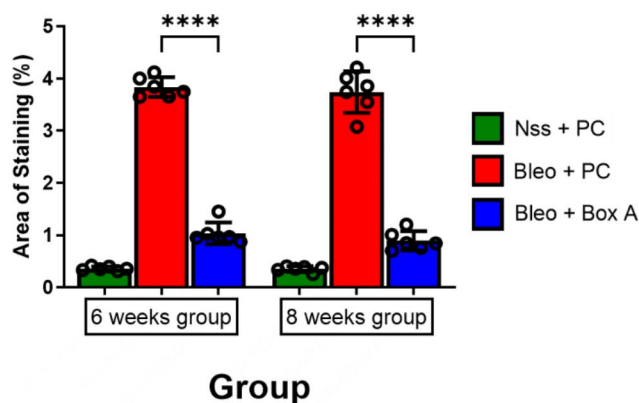


Fig. 2 The effect of Box A on cellular senescence in bleomycin-induced pulmonary fibrosis rats ($n=6$). **(2A)** SA- β -gal staining of rat lung sections. **(2B)** Quantitative analysis of images of SA- β -gal-stained rat lungs. The values represent the means \pm SDs. **** $p \leq 0.0001$ *t*-test

groups that received NSS+plasmid control, bleomycin+plasmid control, or bleomycin+Box A for 8 weeks exhibited senescence areas encompassing $0.35 \pm 0.05\%$, $3.74 \pm 0.40\%$, and $0.89 \pm 0.18\%$ (mean \pm SD) of the total tissue area, respectively.

The calculated p-value of the differences between the groups treated with bleomycin+plasmid control for 6 weeks and with bleomycin+Box A for 6 weeks were less than 0.01% (p-value < 0.0001). The calculated p-value of the differences between the groups treated with bleomycin+plasmid control for 8 weeks and with bleomycin+Box A for 8 weeks were also less than 0.01% (p-value < 0.0001).

We also collected blood samples from the rats after Box A was administered to treat the induced pulmonary fibrosis (Supplemental Fig. 1). The Ca-P-coated Box A-producing plasmid was proved to reach the lung tissue, enter the cells, and produce Box A as intended (Supplemental Fig. 2).

Effectiveness of Box A in reducing fibrosis in bleomycin-induced pulmonary fibrosis

We harvested the lung tissue for histopathological staining via Masson-Trichrome staining and analyzed the area of fibrous tissue deposits. We subsequently calculated the area of fibrosis for each group (Fig. 3). The fibrotic tissue areas of the rats in the NSS+plasmid control, bleomycin+plasmid control, and bleomycin+Box A groups after 6 weeks were $3.25 \pm 0.97\%$, $18.60 \pm 1.49\%$, and $3.58 \pm 1.11\%$ (mean \pm SD) of the total area, respectively. For the groups that received NSS+plasmid control, bleomycin+plasmid control, or bleomycin+Box A for 8 weeks, the fibrotic areas were $3.05 \pm 0.52\%$, $18.74 \pm 1.66\%$, and $4.11 \pm 1.36\%$ (mean \pm SD), respectively.

The calculated p-value of the differences between the groups treated with bleomycin+plasmid control for 6 weeks and with bleomycin+Box A for 6 weeks were less than 0.01% (p-value < 0.0001). The calculated p-value of the differences between the groups treated with bleomycin+plasmid control for 8 weeks and with bleomycin+Box A for 8 weeks were less than 0.01% (p-value < 0.0001).

Effectiveness of Box A on surfactant protein C production in bleomycin-induced pulmonary fibrosis

After our treatment of bleomycin-induced pulmonary fibrosis in the rats with Box A protein following our experimental protocol, we sacrificed the rats and harvested the lung tissue for anti-sftpc (anti-surfactant protein C) immunohistostaining and analyzed the area of staining (Fig. 4). We calculated the area of surfactant protein C for each group as follows. The groups that received NSS+plasmid control, bleomycin+plasmid control, or bleomycin+plasmid control for 6 weeks exhibited

surfactant protein C areas representing $13.71 \pm 2.64\%$, $3.44 \pm 0.96\%$, and $2.52 \pm 1.38\%$ (mean \pm SD) of the total tissue area, respectively. The groups that received NSS+plasmid control, bleomycin+plasmid control, or bleomycin+plasmid control for 8 weeks exhibited surfactant protein C areas representing $13.01 \pm 1.55\%$, $3.60 \pm 1.68\%$, and $6.82 \pm 0.65\%$ (mean \pm SD) of the total tissue area, respectively.

The calculated p-value of the differences between the groups treated with bleomycin+plasmid control for 6 weeks and bleomycin+Box A for 6 weeks were 26.06% (p-value = 0.2606). The calculated p-value of the differences between the groups treated with bleomycin+plasmid control for 8 weeks and with bleomycin+Box A for 8 weeks were 0.39% (p-value = 0.0039).

Discussion

Our research demonstrated that administering the Box A-producing plasmid to rats with bleomycin-induced pulmonary fibrosis significantly reduced the number of senescent cells and fibrotic deposit areas in the rat lung tissue within 6 to 8 weeks compared with those in the control group. The results also revealed a significant improvement in surfactant protein production, although this was seen at only the 8-week time point and did not ultimately return to baseline levels.

Regarding how Box A helps reduce senescence, our team has recently published research findings about the mechanism involved [14, 24–26]. To summarize, the administered plasmid produces a Box A portion of the HMGB1 protein, and these Box A proteins then spread throughout the cells. Some Box A transfers into the cell nucleus, promoting DNA stabilization, DNA stress relief, and DNA protection by DNA gap production. Once senescent cells or pre-senescent cells have received sufficient Box A and achieved DNA stabilization, these cells reduce the DNA damage response and consequently emerge from the senescent state and return to normal.

Box A clearing fibrosis may be due to a reduction in the number of senescent cells. After Box A reversed the senescent phenotype, these cells began functioning normally. These rejuvenated cells include fibrocytes, fibroblasts, and tissue-specific macrophages. These cells create, organize, retain, and destroy fibrotic tissue [27–29]. The fibroblasts and fibrocytes usually create and re-arrange fibers into regular configurations when these cells function correctly. Senescent cells, however, organize connective tissue in the wrong direction, causing fibrosis. After the fibroblasts rejuvenate, they now produce only the correctly re-arranged fibers. The fibrous material degrades through normal cellular function. For example, fibrous is destroyed by tissue-specific macrophages. Senescent macrophages, on the other hand, cannot get rid of the fibrous properly. Therefore,

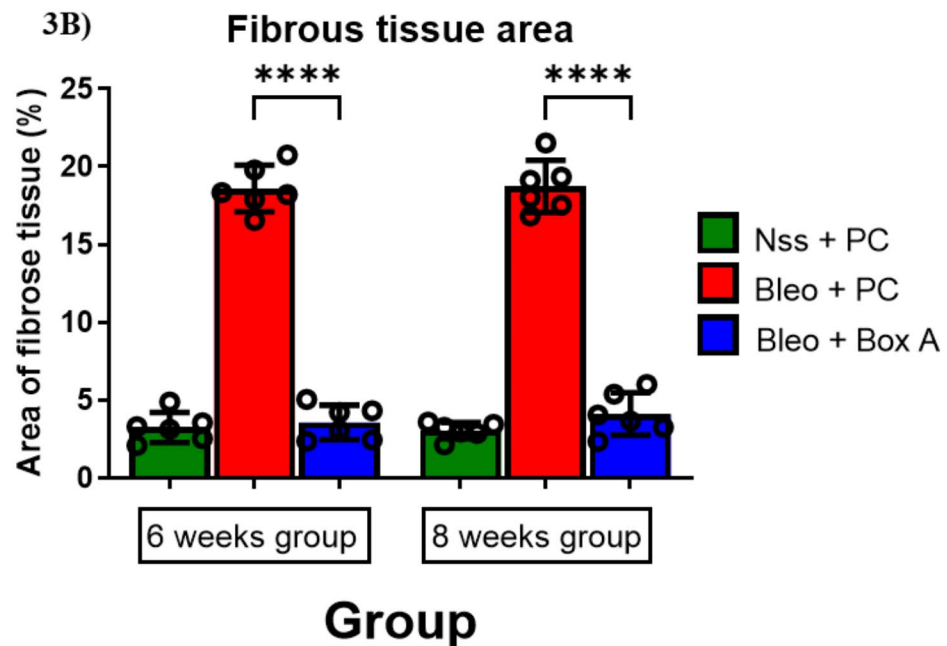
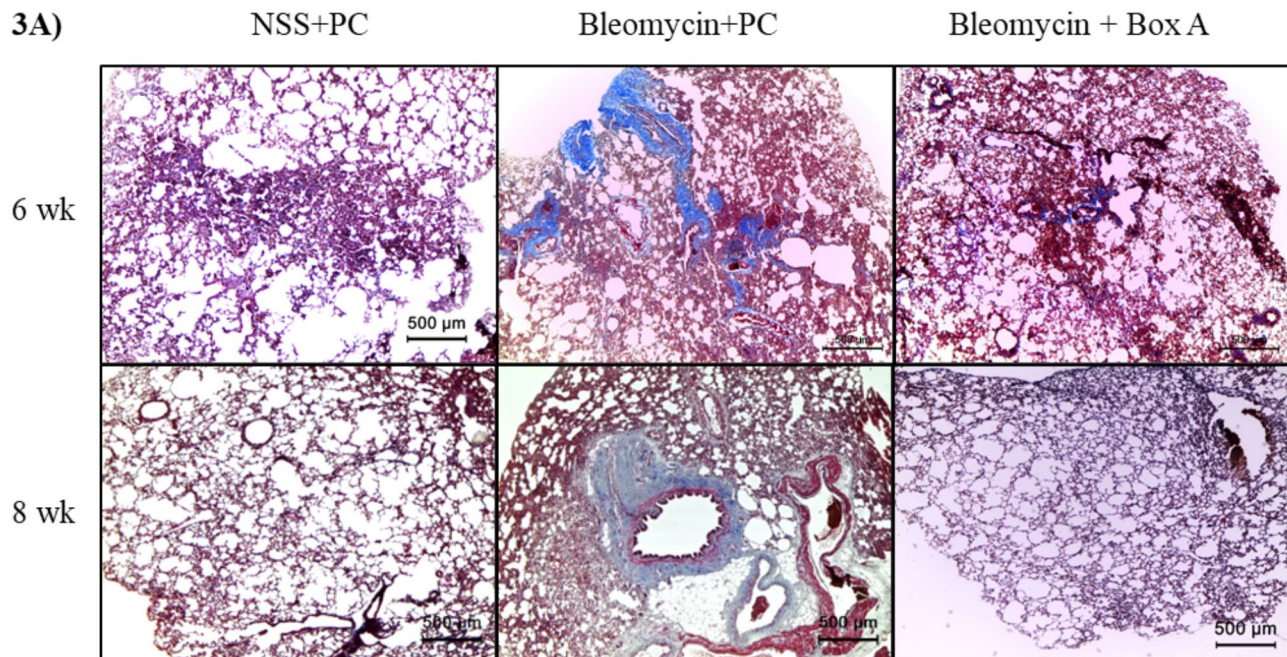


Fig. 3 Effect of Box A on fibrotic tissue deposits in bleomycin-induced pulmonary fibrosis rats ($n=6$). Masson-Trichrome staining of rat lung sections (3A). Quantitative analysis of pictures of Masson-Trichrome-stained rat lungs (3B). The values represent the means \pm SDs. **** $p \leq 0.0001$ t-test

rejuvenating fibrocytes, fibroblasts, and tissue-specific macrophages would produce corrected connective tissue and abolish fibrosis.

With respect to the ability of Box A to promote surfactant protein production, the rejuvenated cells include not only fibroblasts and macrophages inside the tissue, Box A also affects all cells, including epithelial cells and tissue progenitor cells [30–31]. When senescent epithelial cells rejuvenate, their protein-producing function returns to

normal. Therefore, epithelial cells can re-produce normal surfactant protein [32–33]. Additionally, as progenitor cells return to normal, they enter the cell cycle and differentiate to replace destroyed epithelial cells in the tissue [34]. Because cell division and cell differentiation require time, surfactant protein production is slower than rejuvenation and fibrosis clearance.

Regarding translating Box A as the treatment from the rat animal model to the treatment for human

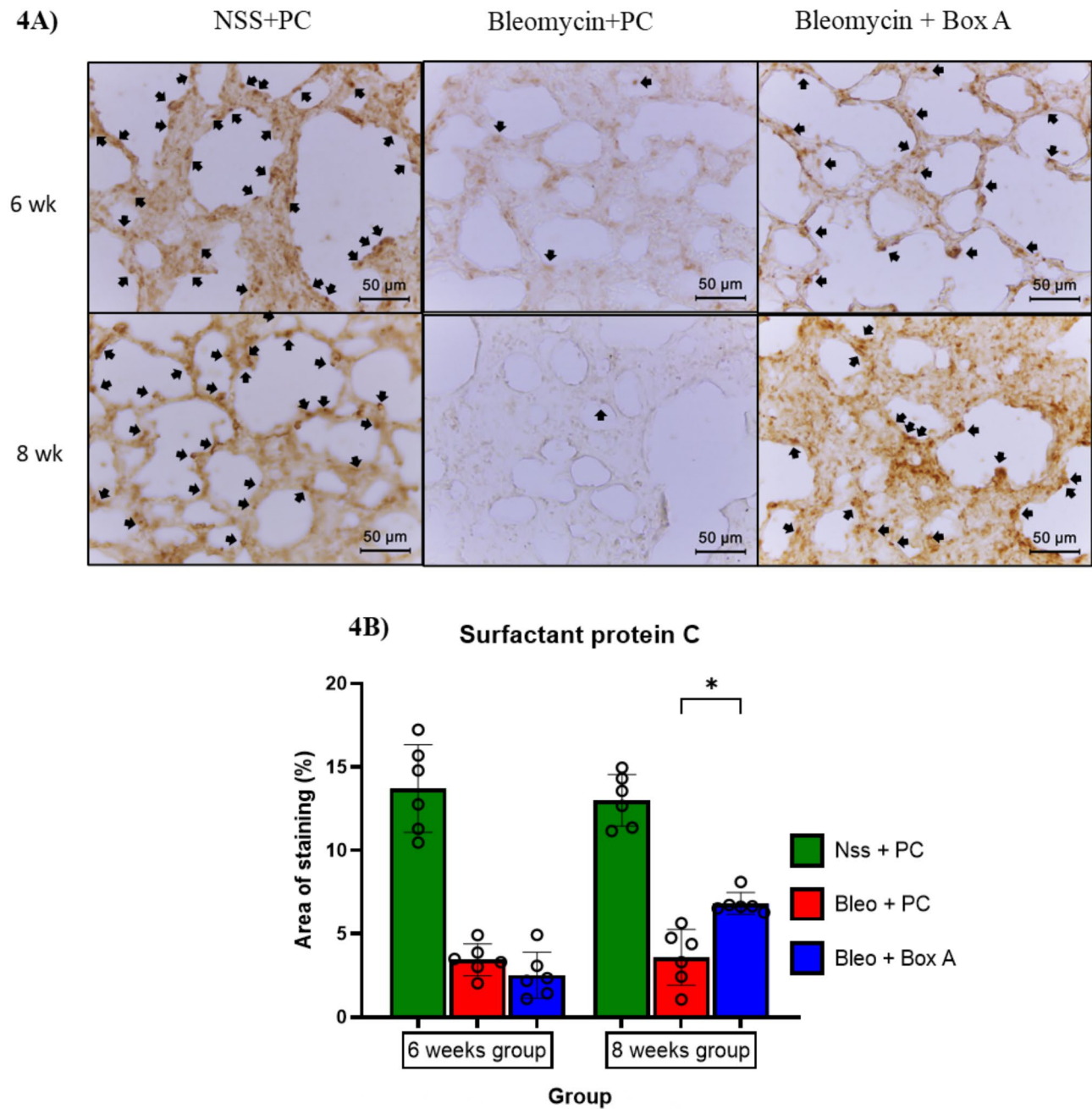


Fig. 4 The effect of Box A on surfactant protein C production in bleomycin-induced pulmonary fibrosis rats ($n=6$). **(4A)** Immunohistostaining with an anti-sftpc antibody in rat lung sections. **(4B)** Quantitative analysis of the images of immunohistostaining in the rat lung. The positive staining is the area with brown hue with some are clump up to form a darker brown spot (pointed by the black arrow). While the negative staining would be the area with transparent white as shown very prominent in the Bleomycin + PC group of both 6 and 8 week. The values represent the means \pm SDs. $*p \leq 0.05$

pulmonary fibrosis, we need to consider the pathogenesis of the disease so that Box A can offer an adequate treatment. The pulmonary fibrosis type that would benefit from Box A would be the disease whose pathogenesis involves HMGB1-produced DNA gap reduction, such as prolonged DNA damages by drug or radiation or any cellular environments promoting HMGB1 release.

If pathogenesis bypasses HMGB1-produced DNA gap reduction, Box A should not provide long-term benefits. Nevertheless, Box A can be used to test a variety of etiologic factors, such as genetic defects of surfactant protein, an autoimmune disease, or idiopathic, or Post-COVID-19 syndrome [35], and determine whether or not

youth-DNA-gap reduction is involved in the pathogenesis of the diseases.

Conclusions

As pulmonary fibrosis continues to be an incurable disease, finding or developing novel and effective treatment is essential. Pulmonary fibrosis in humans has multiple etiologies. An examination of the effect of Box A gene therapy in treating bleomycin-induced pulmonary fibrosis in a rat model revealed that Box A gene therapy could treat pulmonary fibrosis by reducing the number of senescent cells in the diseased tissue, reducing the fibrotic tissue area and increasing surfactant protein production and the abolishment of fibrous tissue due to rejuvenation confirmed that HMGB1-produced-DNA-gap reduction-DNA damage-cellular senescence cascade is mainstream pathogenesis of the pulmonary fibrosis model. Also, this experiment shows that Box A is as effective as the previous two age-induced liver fibrosis experiments. Future clinical trials should test each type of pulmonary fibrosis disease and determine whether or not Box A will be a helpful remedy. Moreover, the ability of Box A to help rejuvenate senescent cells and help cure pulmonary fibrosis should be an example for future research and the development of new treatments for other pathogenesis driven by cellular senescence.

Abbreviations

anti-sftPC	Anti - surfactant protein C
Ble	Bleomycin
Box A	Box A portion of the high mobility group Box 1 protein
BUN	Blood urea nitrogen
Ca-P	Calcium Phosphate
IHC	Immunohistochemistry
i.p.	Intraperitoneally
NSS	Normal saline solution
OCT	Optimal cutting temperature
PC	Plasmid control
SA-β-Gal	Senescence associated - beta - galactosidase

Supplementary Information

The online version contains supplementary material available at <https://doi.org/10.1186/s12890-025-03522-2>.

Supplementary Material 1

Acknowledgements

The authors thank Assistant Professor Amornpun Sereemasun, MD PhD, for providing ethics and methodology guidance, especially pertaining to the animal model, tissue processing and histology staining.

Author contributions

R.P., S.Y. and A.M. conceived the study and designed the analysis; R.P. and S.Y. designed the methodology and investigation; R.P. analyzed and wrote the original draft of the paper and the animal care and use protocol; S.Y. reviewed and edited the animal care and use protocol; A.M. supplied grant support. A.M. and S.Y. reviewed and edited the article; R.P. and S.C. handled the animals; A.M. and S.Y. are involved in supervision and visualization; and all authors read and approved the final manuscript.

Funding

This work was supported by the Applied Research of Rejuvenating DNA by Genomic Stability Molecule (REDGEM) for the treatment of age-associated disease. National Research Council of Thailand (NRCT), the National Science and Technology Development Agency, Thailand [Research Chair Grant, P-19-50189].

Data availability

The authors declare that the data supporting the findings of this study are available within the paper, and its supplementary information files. The full length of human HMGB1 DNA sequence used during the current study is available in the GenBank Nucleotide Repository, accession number: BT020159.

Declarations

Ethics approval and consent to participate

All the animal procedures were reviewed and approved by the Animal Care and Use Committee, Medical Faculty, Chulalongkorn University, Thailand, in accordance with the Association for Assessment and Accreditation of Laboratory Animal Care (AAALAC) guidelines (Approval No. 032/2564).

Consent for publication

Not applicable.

Competing interests

The authors declare no competing interests.

Clinical trial number

Not applicable.

ARRIVE guidelines statement

The authors confirm that the study is in accordance with ARRIVE guidelines.

Received: 15 October 2024 / Accepted: 23 January 2025

Published online: 31 January 2025

References

1. Barratt SL, Creamer A, Hayton C, Chaudhuri N. Idiopathic pulmonary fibrosis (IPF): an overview. *J Clin Med*. 2018;7(8):201. <https://doi.org/10.3390/jcm7080201>.
2. Krishna R, Chapman K, Ullah S. Aug. Idiopathic Pulmonary Fibrosis. [Updated 2023 Jul 31]. In: StatPearls [Internet]. Treasure Island (FL): StatPearls Publishing; 2023 Jan. Accessed 5 2024. <https://www.ncbi.nlm.nih.gov/books/NBK448162/>
3. Zisman DA, Keane MP, Belperio JA, Strieter RM, Lynch JP III. Pulmonary fibrosis. *Methods Mol Med*. 2005;117:3–44. <https://doi.org/10.1385/1-59259-940-003>.
4. Zheng Q, Cox IA, Campbell JA, Xia Q, Otahal P, de Graaff B, Corte TJ, Teoh AKY, Walters EH, Palmer AJ. Mortality and survival in idiopathic pulmonary fibrosis: a systematic review and meta-analysis. *ERJ Open Res*. 2022;8(1):00591–2021. <https://doi.org/10.1183/23120541.00591-2021>.
5. Wynn TA. Integrating mechanisms of pulmonary fibrosis. *J Exp Med*. 2011;208(7):1339–50. <https://doi.org/10.1084/jem.20110551>.
6. Bringardner BD, Baran CP, Eubank TD, Marsh CB. The role of inflammation in the pathogenesis of idiopathic pulmonary fibrosis. *Antioxid Redox Signal*. 2008;10(2):287–301. <https://doi.org/10.1089/ars.2007.1897>.
7. Parimon T, Hohmann MS, Yao C. Cellular senescence: pathogenic mechanisms in lung fibrosis. *Int J Mol Sci*. 2021;22(12):6214. <https://doi.org/10.3390/ijms22126214>.
8. Zhu J, Liu L, Ma X, Cao X, Chen Y, Qu X, Ji M, Liu H, Liu C, Qin X, Xiang Y. The role of DNA damage and repair in idiopathic pulmonary fibrosis. *Antioxid (Basel)*. 2022;11(11):2292. <https://doi.org/10.3390/antiox11112292>.
9. Sgalla G, Iovene B, Calvello M, Ori M, Varone F, Richeldi L. Idiopathic pulmonary fibrosis: pathogenesis and management. *Respir Res*. 2018;19(1):32. <https://doi.org/10.1186/s12931-018-0730-2>.
10. Wilson MS, Wynn TA. Pulmonary fibrosis: pathogenesis, etiology and regulation. *Mucosal Immunol*. 2009;2(2):103–21. <https://doi.org/10.1038/mi.2008.85>.

11. Raghu G, Collard HR, Egan JJ, Martinez FJ, Behr J, Brown KK, Colby TV, Cordier JF, Flaherty KR, Lasky JA, Lynch DA, Ryu JH, Swigris JJ, Wells AU, Ancochea J, Bourros D, Carvalho C, Costabel U, Ebina M, Hansell DM, ATS/ERS/JRS/ALAT Committee on Idiopathic Pulmonary Fibrosis. An official ATS/ERS/JRS/ALAT statement: idiopathic pulmonary fibrosis: evidence-based guidelines for diagnosis and management. *Am J Respir Crit Care Med*. 2011;183(6):788–824. <https://doi.org/10.1164/rccm.2009-040GL>.
12. Moore BB, Lawson WE, Oury TD, Sisson TH, Raghavendran K, Hogaboam CM. Animal models of fibrotic lung disease. *Am J Respir Cell Mol Biol*. 2013;49(2):167–79. <https://doi.org/10.1165/rcmb.2013-0094TR>.
13. Cheresch P, Kim SJ, Tulasiram S, Kamp DW. Oxidative stress and pulmonary fibrosis. *Biochim Biophys Acta*. 2013;1832(7):1028–40. <https://doi.org/10.1016/j.bbadis.2012.11.021>.
14. Yasom S, Watcharanurak P, Bhummaphan N, Thongsroy J, Puttanyalears C, Settayanon S, Chalertpet K, Khumsri W, Kongkaew A, Patchsung M, Siriwatanakankul C, Pongpanich M, Pin-On P, Jindatip D, Wanotayan R, Odton M, Supasai S, Oo TT, Arunsak B, Pratchayasakul W, Mutirangura A. The roles of HMGB1-produced DNA gaps in DNA protection and aging biomarker reversal. *FASEB Bioadv*. 2022;4(6):408–34. <https://doi.org/10.1096/fba.2021-00131>.
15. Yasom S, Khumsri W, Boonsongserm P, Kitkumthorn N, Ruangvejvorachai P, Sooksamran A, Wanotayan R, Mutirangura A. B1 siRNA increases de novo DNA methylation of B1 elements and promotes wound healing in diabetic rats. *Front Cell Dev Biol*. 2022;9:802024. <https://doi.org/10.3389/fcell.2021.802024>.
16. Faul F, Erdfelder E, Lang AG, Buchner A. G*Power 3: a flexible statistical power analysis program for the social, behavioral, and biomedical sciences. *Behav Res Methods*. 2007;39(2):175–91. <https://doi.org/10.3758/BF03193146>.
17. Turgut HN, Kara H, Elagoz S, Deveci K, Gungor H, Arslanbas E. The protective effect of naringin against bleomycin-induced pulmonary fibrosis in Wistar rats. *Pulm Med*. 2016;2016:7601393. <https://doi.org/10.1155/2016/7601393>.
18. Hübner RH, Gitter W, El Mokhtari NE, Mathiak M, Both M, Bolte H, Freitag-Wolf S, Bewig B. Standardized quantification of pulmonary fibrosis in histological samples. *Biotechniques*. 2008;44(4):507–511, 514–517. <https://doi.org/10.2144/000112729>.
19. Razaque M, Hossain M, Kohno S, et al. Bleomycin-induced pulmonary fibrosis in rat is associated with increased expression of collagen-binding heat shock protein (HSP) 47. *Virchows Arch*. 1998;432(5):455–60. <https://doi.org/10.1007/s004280050191>.
20. Thrall RS, et al. Bleomycin-induced pulmonary fibrosis in the rat: inhibition by indomethacin. *Am J Pathol*. 1979;95(1):117–30.
21. Muggia FM, Louie AC, Sikic BI. Pulmonary toxicity of antitumor agents. *Cancer Treat Rev*. 1983;10(4):221–43. [https://doi.org/10.1016/0305-7372\(83\)90012-9](https://doi.org/10.1016/0305-7372(83)90012-9).
22. El-Medany A, Hagar HH, Moursi M, At Muhammed R, El-Rakhawy FI, El-Medany G. Attenuation of bleomycin-induced lung fibrosis in rats by mesna. *Eur J Pharmacol*. 2005;509(1):61–70. <https://doi.org/10.1016/j.ejphar.2004.12.01>.
23. Gamad N, Malik S, Suchal K, et al. Metformin alleviates bleomycin-induced pulmonary fibrosis in rats: pharmacological effects and molecular mechanisms. *Biomed Pharmacother*. 2018;97:1544–53. <https://doi.org/10.1016/j.biopha.2017.11.101>.
24. Ei ZZ, Mutirangura A, Arunmanee W, Chanvorachote P. The Role of Box A of HMGB1 in Enhancing Stem Cell Properties of Human Mesenchymal Cells: A Novel Approach for the Pursuit of Anti-aging Therapy. *In Vivo*. 2023;37(5):2006–2017. <https://doi.org/10.21873/invivo.13298>
25. Ferreira JN, Bhummaphan N, Chaisuparat R, et al. Unveiling senescence-associated ocular pathogenesis via lacrimal gland organoid magnetic bioassembly platform and HMGB1-Box A gene therapy. *Sci Rep*. 2024;14:21784. <https://doi.org/10.1038/s41598-024-73101-8>.
26. Watcharanurak P, Mutirangura A. Genome wide hypomethylation and youth-associated DNA gap reduction promoting DNA damage and senescence-associated pathogenesis. *Med Res Arch*. 2023;11(12). <https://doi.org/10.18103/mra.v11i12.4952>.
27. Keeley EC, Mehrad B, Strieter RM. Fibrocytes: bringing new insights into mechanisms of inflammation and fibrosis. *Int J Biochem Cell Biol*. 2010;42(4):535–42. <https://doi.org/10.1016/j.biocel.2009.10.014>.
28. Su L, Dong Y, Wang Y, et al. Potential role of senescent macrophages in radiation-induced pulmonary fibrosis. *Cell Death Dis*. 2021;12:527. <https://doi.org/10.1038/s41419-021-03811-8>.
29. Hyun J, Eom J, Im J, Kim YJ, Seo I, Kim SW, Im GB, Kim YH, Lee DH, Park HS, Yun DW, Kim DI, Yoon JK, Um SH, Yang DH, Bhang SH. Fibroblast function recovery through rejuvenation effect of nanovesicles extracted from human adipose-derived stem cells irradiated with red light. *J Control Release*. 2024;368:453–65. <https://doi.org/10.1016/j.jconrel.2024.02.047>.
30. Parimon T, Chen P, Stripp BR, Liang J, Jiang D, Noble PW, Parks WC, Yao C. Senescence of alveolar epithelial progenitor cells: a critical driver of lung fibrosis. *Am J Physiol Cell Physiol*. 2023;325(2):C483–95. <https://doi.org/10.1152/ajpcell.00239.2023>.
31. Yao C, Guan X, Carraro G, Parimon T, Liu X, Huang G, Mulay A, Soukiasian HJ, David G, Weigt SS, Belperio JA, Chen P, Jiang D, Noble PW, Stripp BR. Senescence of alveolar type 2 cells drives progressive pulmonary fibrosis. *Am J Respir Crit Care Med*. 2021;203(6):707–17. <https://doi.org/10.1164/rccm.202004-1274OC>.
32. Schafer M, White T, Iijima K, et al. Cellular senescence mediates fibrotic pulmonary disease. *Nat Commun*. 2017;8:14532. <https://doi.org/10.1038/ncomms14532>.
33. Yamada Z, Nishio J, Motomura K, Mizutani S, Yamada S, Mikami T, Nanki T. Senescence of alveolar epithelial cells impacts initiation and chronic phases of murine fibrosing interstitial lung disease. *Front Immunol*. 2022;13:935114. <https://doi.org/10.3389/fimmu.2022.935114>.
34. Zeng L, Yang XT, Li HS, Li Y, Yang C, Gu W, Zhou YH, Du J, Wang HY, Sun JH, Wen DL, Jiang JX. The cellular kinetics of lung alveolar epithelial cells and its relationship with lung tissue repair after acute lung injury. *Respir Res*. 2016;17(1):164. <https://doi.org/10.1186/s12931-016-0480-y>.
35. Mohiuddin M, Kasahara K. Cellular senescence is a potential severity factor for COVID-19: suitable targets required to eliminate cellular senescence. *Respir Med*. 2021;186:106517. <https://doi.org/10.1016/j.rmed.2021.106517>.

Publisher's note

Springer Nature remains neutral with regard to jurisdictional claims in published maps and institutional affiliations.